Identification of a novel FOXO3-associated prognostic model in hepatocellular carcinoma

SONGMEI GUAN[1], QIANG LIN[2], PEIWU HUANG[2], KANGQIANG LIN[2] and SHIGANG DUAN[2]

[1]Department of Clinical Pharmacy, Second Affiliated Hospital of Guangdong Medical University, Zhanjiang, Guangzhou 524003, P.R. China; [2]Department of Hepatobiliary Surgery, Second Affiliated Hospital of Guangdong Medical University, Zhanjiang, Guangzhou 524003, P.R. China

Received July 4, 2024; Accepted February 14, 2025

DOI: 10.3892/ol.2025.14976

Abstract. Although numerous molecular classifications are available to predict the prognosis of patients with hepatocellular carcinoma (HCC), they are still unsatisfactory. Forkhead box O3 (FOXO3) has been widely reported as a transcription factor involved in human cancers, but its role in HCC remains controversial. The present study aimed to explore the role of FOXO3 in HCC, as well as to identify biomarkers and construct prognostic models based on FOXO3. FOXO3 was highly expressed in HCC and was closely associated with poor prognosis in The Cancer Genome Atlas (the training set) and International Cancer Genome Consortium (the validation set). Subsequently, a co-expression network indicated that the red modules were closely related to FOXO3. Five key FOXO3-related genes [DEAD-box helicase 55 (DDX55), RAB10, member RAS oncogene family (RAB10), RAB7A, TATA-box binding protein associated factor, RNA polymerase I subunit B (TAF1B) and TAF3] were obtained using Cox-least absolute shrinkage and selection operator analyses. The 5-gene signature successfully predicted the prognosis of patients with HCC in both the training and validation sets. Enrichment analysis suggested marked differences in AKT and cell cycle-related (E2F targets and G_2/M checkpoints) pathways between HCC subgroups. Furthermore, the tumor microenvironment analysis suggested that the difference in the distribution of M2 macrophages among various subgroups may contribute to the poor prognosis using the CIBERSORTx framework. Furthermore, the mRNA and protein expressions of DDX55, RAB10, RAB7A, TAF1B and TAF3 were found to be higher in HCC tissues compared with paracancerous tissues using RT-qPCR and western blotting. Additionally, knockdown of RAB10, RAB7A and TAF3 inhibited proliferation of Huh7 cells, assessed by a Cell Counting Kit-8 assay. In conclusion, a novel FOXO3-related model was constructed and revealed that RAB10, RAB7A and TAF3 may be potential molecular targets or biomarkers for HCC.

Introduction

Hepatocellular carcinoma (HCC) is a malignant disease with the sixth highest incidence and the third highest mortality worldwide (1). The crucial reasons for the high mortality of HCC include difficulty in early diagnosis, tumor heterogeneity and poor efficacy of late stage treatment (2). Tumor heterogeneity includes both the heterogeneity of tumor cells and the tumor microenvironment (3). An increasing number of studies have reported that the heterogeneity of HCC is at the forefront of malignant tumors and has a profound impact on the prognosis and treatment of HCC (3,4). In addition, studies based on bioinformatics analysis of molecular typing and prognostic prediction of HCC have emerged and demonstrated clinical potential (4-6). Unfortunately, the progression of HCC is a multifactor, multistage and constantly changing process due to its heterogeneity, which leads to certain limitations of the models (7). Therefore, it is necessary to explore the novel molecular subtypes and models of HCC for evaluating prognosis.

Forkhead box O3 (FOXO3), a member of the Forkhead box (Fox) transcription factors, is named for its highly conserved DNA-binding domain (DBD) (8). In addition to the DBD, FOXO3 has three other functional domains: a nuclear export signal, a nuclear localization signal and a transactivation domain (9). In the 1990s, FOXO3 was demonstrated to be present at sites of chromosomal translocations, creating oncogenic fusions with the DNA-binding moiety of either paired box gene 3/7 or lysine methyltransferase 2A (10,11). Previous

Correspondence to: Professor Shigang Duan, Department of Hepatobiliary Surgery, Second Affiliated Hospital of Guangdong Medical University, 12 Minyou Road, Xiashan, Zhanjiang, Guangzhou 524003, P.R. China
E-mail: shigang_duan@163.com

Abbreviations: HCC, hepatocellular carcinoma; FOXO3, Forkhead box O3; TCGA, The Cancer Genome Atlas; ICGC, International Cancer Genome Consortium; DBD, DNA-binding domain; WGCNA, weighted correlation network analysis; LASSO, least absolute shrinkage and selection operator; MM, module membership; GS, gene significance; PPI, protein-protein interaction; RS, risk score; ROC, receiver operating characteristic; GSEA, gene set enrichment analysis

Key words: hepatocellular carcinoma, Forkhead box O3, prognosis, biomarkers, bioinformatics

studies have shown that the FOX protein is a tumor suppressor that is often inactivated in cancer (12-14). Gene-editing mouse models have confirmed that knocking out FOXO3 causes hemangiomas (14). Reactivation of FOXO3 by drugs (metformin and SN-38) also mediates the transformation of ovarian and breast cancer cells into non-cancer cells (15). These phenotypes indicate that FOXO3 may have an antitumor role. Currently, the role of FOX3O in HCC seems to be controversial. On the one hand, knockdown of FOXO3 inhibits HCC cell proliferation and promotes HCC cell apoptosis via BNIP3 inhibition (16,17). On the other hand, ursolic acid inhibits HCC cell proliferation by upregulating FOXO3 expression while low expression of FOXO3 augments autophagic flux, promoting sorafenib resistance of HCC cells (18,19). These studies suggest that FOXO3 may serve a different role in HCC from other tumors.

The present study aimed to explore the role of FOXO3 in HCC, construct a novel prognostic model and identify biomarkers for HCC prognosis. To accomplish these aims, The Cancer Genome Atlas (TCGA) and International Cancer Genome Consortium (ICGC) databases were used and weighted correlation network analysis (WGCNA) analysis was used to screen FOXO3-related genes. Subsequently, univariate Cox-least absolute shrinkage and selection operator (LASSO) analysis was used to identify signatures and construct a novel prognostic model. Furthermore, clinical samples of patients with HCC were used to assess mRNA and protein expression of DEAD-box helicase 55 (DDX55), RAB10, member RAS oncogene family (RAB10), RAB7A, TATA-box binding protein associated factor, RNA polymerase I subunit B (TAF1B) and TAF3. Finally, a Cell Counting Kit-8 (CCK-8) assay was used to evaluate the effect of RAB10, RAB7A and TAF3 on proliferation of Huh7 cells.

Materials and methods

Data collection and processing. The RNA-sequencing (RNA-Seq) transcriptome profile (TCGA- LIHC) of transcripts per kilobase of exon model per million mapped reads format, including 365 HCC tissues and 50 normal hepatic tissues, were acquired from TCGA database (TCGA-LIHC, https://portal.gdc.cancer.gov) using the TCGAbiolinks package ((https://bioconductor.org/p-ackages/release/bioc/html/TCGAbiolinks.html, version 2.28.4) (20) in R (version 4.3). The accompanying clinical information of 365 patients with HCC was also obtained by the TCGAbiolinks package in R (version 4.3). For duplicate samples, the mean was calculated and used as the final sample gene expression value. Samples clearly identified as HCC were included and samples with missing or incomplete clinical information [age, sex, tumor, node, metastasis (TNM) staging, survival time and status] were removed in subsequent prognostic and modeling analyses. The patients were then divided into high- and low-FOXO3 expression groups according to X-tile software (version 3.6.1, /x-tile.software.informer.com/), with a cut-off value of 4.206.

The RNA-seq transcriptome data and corresponding clinical information of 206 patients with HCC (ICGC-LIRI-JP), including 206 HCC tissues and 177 normal hepatic tissues, were downloaded from the ICGC database (ICGC-LIRI-JP, https://dcc.icgc.org/). The data from ICGC was processed in the same way as the aforementioned database.

WGCNA. An mRNA co-expression network of the TCGA-LIHC dataset was constructed using the WGCNA R package (version1 73) (21). Briefly, the Pearson correlation between each pair of genes was calculated and the similarity matrix was acquired. The power function was used to transform the similarity matrix to an adjacency matrix using the WGCNA R package and the β was determined through the scale-free topological fit test for constructing scale-free weighted network. A threshold of R^2>0.9 (soft threshold=32) was selected to acquire a high-confidence scale free network. Co-expression modules were acquired through the pairwise topological overlap between genes and highly correlated modules were further merged. The hub module was designated as that with the highest Pearson correlation coefficient and P<0.05. Furthermore, module membership (MM) and gene significance (GS) were calculated and genes with MM >0.8 and GS >0.2 in the hub module were selected as the hub genes.

LASSO regression analysis and protein-protein interaction (PPI) network. LASSO regression analysis was performed using the glmnet (version 4.1-4) (22) and survival (version 3.8-3) (23) R packages. LASSO was then used to identify the final gene signature for constructing the prognostic model according to the minimum λ value. The PPI network was constructed using the STRING database (version 12.0; string-db.org/) and visualized by Cytoscape (version 3.9.1, https://cytoscape.org/).

Construction and validation of the prognostic model. Univariate Cox analysis was used to identify the hub genes and genes with P<0.05 were retained for subsequent analysis. LASSO analysis was performed and five genes were identified for constructing the model according to the minimum λ value (24). The risk score (RS) of each HCC sample was calculated using the following formula: $RS= \Sigma_{i=1}^{n} coef(gene^i) \times expr(gene^i)$. The patients were then divided into high- and low-risk groups according to X-tile software.

Clinical potential evaluation of the prognostic model. Time-dependent receiver operating characteristic (ROC) curves were generated using the pROC R package (version 1.18.5) (25). Univariate and multivariate Cox analyses were performed and visualized using the survival R package, SPSS (version 23; IBM Corp.) and the ggplot2 R package (version 3.5.1) (26). Nomogram and calibration curves were generated using the rms R package (version 7.0) (27).

Gene set enrichment analysis (GSEA) and immune analysis. GSEA of the training (TCGA cohort) and validation sets (ICGC cohort) was performed using GSEA software (version 4.3.2, gsea-msigdb.org/gsea/index.jsp). Hallmark gene sets from the molecular signature database (MSigDB; http://www.gseamsigd-b.org/gsea/msigdb/index.jsp) were defined as the reference gene set database. Pathways with P<0.05 and false discovery rate (FDR) <0.25 were considered statistically different between the high- and low-risk groups. Infiltration of 22 immune cell types in the tumor microenvironment was

analyzed using the CIBERSORTx website (cibersortx.stanford.edu/). Results were visualized using the ggplot2 package.

Reverse transcription-quantitative polymerase chain reaction (RT-qPCR). A total of 10 paired tumor and tumor-adjacent tissues from patients with HCC were collected by hepatectomy between May 2024 and August 2024 from the Second Affiliated Hospital of Guangdong Medical University (Zhanjiang, China). The use of samples was approved by Research Ethics Committee of the Second Affiliated Hospital of Guangdong Medical University (approval no. PJKT-2024-042).

A total of 10 HCC samples obtained were included in accordance with the following inclusion criteria: i) The patient received hepatectomy; ii) all samples were confirmed to have a clinicopathological diagnosis of HCC through pathology reports; and iii) patients had no severe infection and stable vital signs. The exclusion criteria were: i) Patients with secondary and recurrent liver cancer; ii) patients with liver cancer who had received any medication prior to surgery; and iii) patients with multiple primary tumors. The clinical information of 10 patients with HCC is presented the Table SI. Total RNA from HCC and paired paracancerous tissues was extracted using the Total RNA Isolation Kit (cat. no. RE-03011; Foregene Co., Ltd.) according to the manufacturer's instructions. RNA was reverse transcribed to cDNA using a cDNA synthesis kit (cat. no. 1708891; Bio-Rad Laboratories, Inc.) and the following conditions: 5 min at 25˚C, 20 min at 46˚C, 1 min at 95˚C and holding at 4˚C. cDNA was quantified using Universal SYBR Green Supermix (cat. no. 1708891; Bio-Rad Laboratories, Inc.) according to the manufacturer's instructions (denaturation for 5 sec at 95˚C, extension: 30 sec at 60˚C, 40 cycles). Relative mRNA expression was obtained using the $2^{-\Delta\Delta Cq}$ method (28) with GAPDH as the internal reference. The following primers were used: GAPDH forward, 5'-GGAGCGAGATCCCTCCAAAAT-3'; GAPDH reverse, 5'-GGCTGTTGTCATACTTCTCATGG-3'; DDX55 forward, 5'-AGCTGGGCTTCCCGTACAT-3'; DDX55 reverse, 5'-CAGCGACATCTTTGTTTCGCA-3'; RAB10 forward, 5'-CTGCTCCTGATCGGGGATTC-3', RAB10 reverse, 5'-TGATGGTGTGAAATCGCTCCT-3'; RAB7A forward, 5'-GTGTTGCTGAAGGTTATCATCCT-3'; RAB7A reverse, 5'-GCTCCTATTGTGGCTTTGTACTG-3'; TAF1B forward, 5'-AAAGAACGCTGTACTCAGTGTG-3'; TAF1B reverse, 5'-CCCCGGTTGAGGGCTTTTA-3'; TAF3 forward, 5'-ATGTGCGAGAGTTACTCCAGG-3'; and TAF3 reverse, 5'-GGGTCTGTTCGGCCATAGAG-3'.

Western blot analysis. Protein from HCC and paired paracancerous tissues were extracted using radioimmunoprecipitation assay buffer with protease and phosphatase inhibitors (cat. no. P0013C; Beyotime Institute of Biotechnology) according to the manufacturer's instructions. Protein samples were quantification by the BCA kit (cat. no. P0012S, Beyotime Institute of Biotechnology). Protein samples were heated at 70˚C for 10 min after mixing with sodium dodecyl sulfate-polyacrylamide gel electrophoresis (SDS-PAGE) buffer (cat. no. P0015A; Beyotime Institute of Biotechnology) and then added into a pre-prepared 10% gel for electrophoresis (15 μg per lane). The protein was transferred to polyvinylidene fluoride membranes. Subsequently, the membranes were blocked with 5% skim milk at room temperature for 2 h and then incubated with primary antibody at 4˚C overnight. After incubation, the membranes were placed on a shaker and washed with TBST buffer (1 l TBS buffer with 1 ml Tween-20) for 7 min. After washing three times, the membranes were incubated with the secondary antibody at room temperature for 1 h. Finally, the membranes were washed and developed by chemiluminescence. The gray values were obtained by ImageJ (National Institutes of Health, version 1.54h) and analyzed using GraphPad Prism (Dotmatics, version 10.2.3). The following antibodies were used: β-actin (1:1,000; cat. no. ET1702-52; HUABIO), DDX55 (1:1,000; cat. no. ER63225; HUABIO), RAB10 (1:1,000; cat. no. 11808-1-AP; Proteintech Group, Inc.), RAB7A (1:1,500; cat. no. 55469-1-AP; Proteintech Group, Inc.), TAF1B (1:500; cat. no. 12818-1-AP; Proteintech Group, Inc.), FOXO3 (1:1,000; cat. no. A9270; ABclonal Biotech Co., Ltd.) and TAF3 (1:500; cat. no. 18901-1-AP; Proteintech Group, Inc.), HRP conjugated goat anti-rabbit IgG polyclonal antibody (1:30000, HA1001, HUABIO), HRP conjugated goat anti-mouse IgG polyclonal antibody (1:30,000, HA1006, HUABIO).

Cell transfection. The Huh7 cell was obtained from Cell Bank of the Chinese Academy of Sciences (Shanghai, China) and cells (10,000/well) were seeded into 6-well plates. Cells were cultured using DMEM (Gibco, USA) supplemented with 10% FBS) (ScienCell, USA) and 1% penicillin and streptomycin (HyClone). After the cell density reached 20%, the cells were transfected with small interfering RNAs (siRNA; Shanghai GenePharma Co., Ltd.). Briefly, the siRNA, serum-free medium and siRNA-Mate transfer agent (cat. no. G04003; Shanghai GenePharma Co., Ltd.) were mixed, added to the cells at a final concentration of 100 nM and shaken well according to the manufacturer's instructions. After 72 h transfection, the protein was extracted to detect the knockdown efficiency via western blot analysis. The following siRNA sequences were used: RAB10 sense, 5'-CCAUAGGAAUAGACUUCAAGA-3'; antisense, 5'-UUGAAGUCUAUUCCUAUGGUG-3'; RAB7A sense, 5'-GGAAGAAAGUGUUGCUGAAGG-3'; antisense, 5'-UUCAGCAACACUUUCUUCCUA-3'; TAF3 sense, 5'-GCGGGAUGUGCGAGAGUUACU-3'; antisense, 5'-UAACUCUCGCACAUCCCGCUG-3'; FOXO3 sense, 5'-AACUAAACCCUUUAGUGACAU-3'; antisense, 5'-GUCACUAAAGGGUUUAGUUUU-3'; negative control sense, 5'-CAUAAAUCUACAGGAUGAUTT-3'; antisense, 5'-AUCAUCCUGUAGAUUUAUGTT-3'.

CCK-8 assay. The cells (5,000/well) were seeded in 96-well plates with three replicates per group. According to the manufacturer's instructions, the absorbance at 450 nm was detected using a CCK-8 kit after incubation for 2 h (cat. no. ZP328-3; Beijing Zoman Biotechnology Co., Ltd.) at 6, 24, 48 and 72 h after seeding the cells. The absorbance value detected 6 h after seeding the cells was considered as 0 h.

Statistical analysis. Data with normal distribution and skewed distribution was analyzed by t test and Wilcoxon rank-sum test, respectively. The results of the bioinformatics analysis were analyzed using R software (version 4.2.0) and the Wilcoxon rank-sum test. Kaplan-Meier survival curves

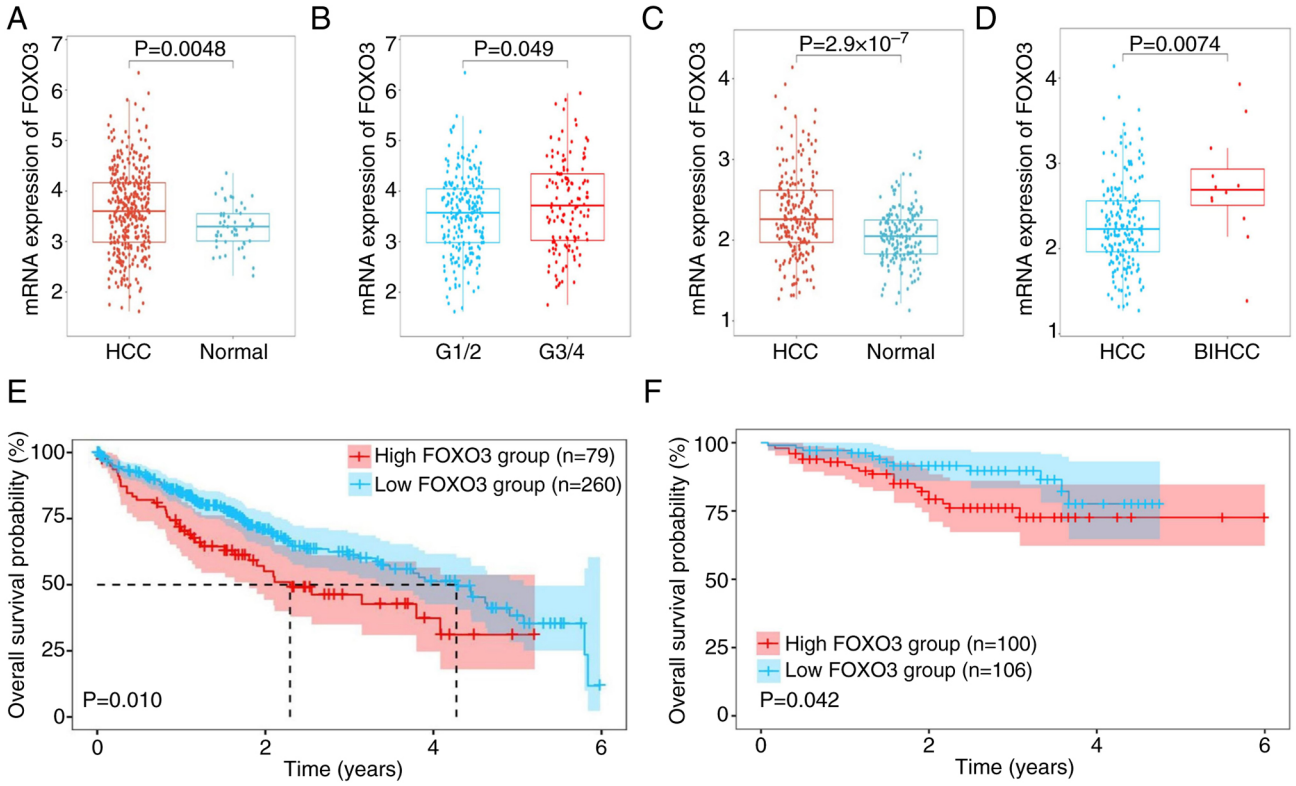

Figure 1. FOXO3 is highly expressed in HCC tissues and associated with poor prognosis. (A) mRNA expression of FOXO3 in HCC and normal tissues from TCGA dataset. (B) mRNA expression of FOXO3 in pathological grading G1/2 and G3/4 from TCGA dataset. (C) mRNA expression of FOXO3 in HCC and normal tissues from the ICGC dataset. (D) mRNA expression of FOXO3 in HCC with or without bile duct invasion from the ICGC dataset. Overall survival in patients with HCC with high or low FOXO3 expression from (E) TCGA and (F) ICGC datasets. FOXO3, Forkhead box O3; HCC, hepatocellular carcinoma; TCGA, The Cancer Genome Atlas; ICGC, International Cancer Genome Consortium; BIHCC, bile duct invasion hepatocellular carcinoma.

were compared using the log-rank test or two-stage method. The survival curves were plotted and cut-off was selected by the survival package in R. The results of RT-qPCR, western blot analysis and CCK-8 assay were analyzed using Student's t-test. All statistical analyses were performed using R, SPSS and GraphPad Prism (version 9.3.1; Dotmatics). P<0.05 was considered to indicate a statistically significant difference.

Results

FOXO3 is highly expressed and associated with poor prognosis in HCC. To evaluate the mRNA expression of FOXO3, the transcriptome and corresponding clinical profiles of 365 patients with HCC and 206 patients with HCC were obtained from TCGA and ICGC-LIRI-JP, respectively. The mRNA expression of FOXO3 in HCC tissues was higher compared with that in normal tissues in the TCGA dataset (Fig. 1A). Moreover, the patients with pathology grade G3/4 had higher expression of FOXO3 compared with grade G1/2 (Fig. 1B), but the mRNA expression of FOXO3 was not associated with TNM staging and vascular invasion (Fig. S1A and B). The ICGC database was used to further validate these findings. FOXO3 expression was significantly higher in HCC tissues compared with normal tissues (Fig. 1C). Moreover, FOXO3 was significantly higher in tissues with expressed in bile duct invasion HCC compared with HCC (Fig. 1D), but the mRNA expression of FOXO3 did not differ with higher TNM staging or with vascular invasion (Fig. S1C and D). Both databases indicate that high expression of FOXO3 was strongly associated with poor prognosis in HCC (Fig. 1E and F).

Identification of the FOXO3-associated gene module in HCC. FOXO3, as a transcription factor, may serve an important role in HCC; therefore, WGCNA was used to identify a FOXO3-associated gene module. A scale-free network was constructed using WGCNA in 365 patients with HCC from TCGA (Fig. 2A). The average-linkage hierarchical clustering method was used to cluster genes and modules with >80% similarity were merged (Fig. 2B), resulting in six modules. The correlations between each module and the mRNA expression of FOXO3 in HCC were analyzed (Fig. 2C), which indicated that the red module was most closely related to FOXO3 (Pearson coefficient of 0.72). The gene distribution in the red module was further analyzed, which demonstrated that GS and MM were significantly correlated, suggesting that genes in the red module were strongly associated with FOXO3 (Fig. 2D).

Identification of FOXO3-associated key gene signature in HCC. Based on the criteria of MM >0.8 and GS >0.2, hub genes in the red module were identified, resulting in 875 hub genes. Univariate Cox regression analysis was then used to screen 294 prognosis-associated genes from 875 genes with a P-value of <0.05 (Fig. 3A). To further narrow the range of variables, LASSO regression analysis was performed, which identified

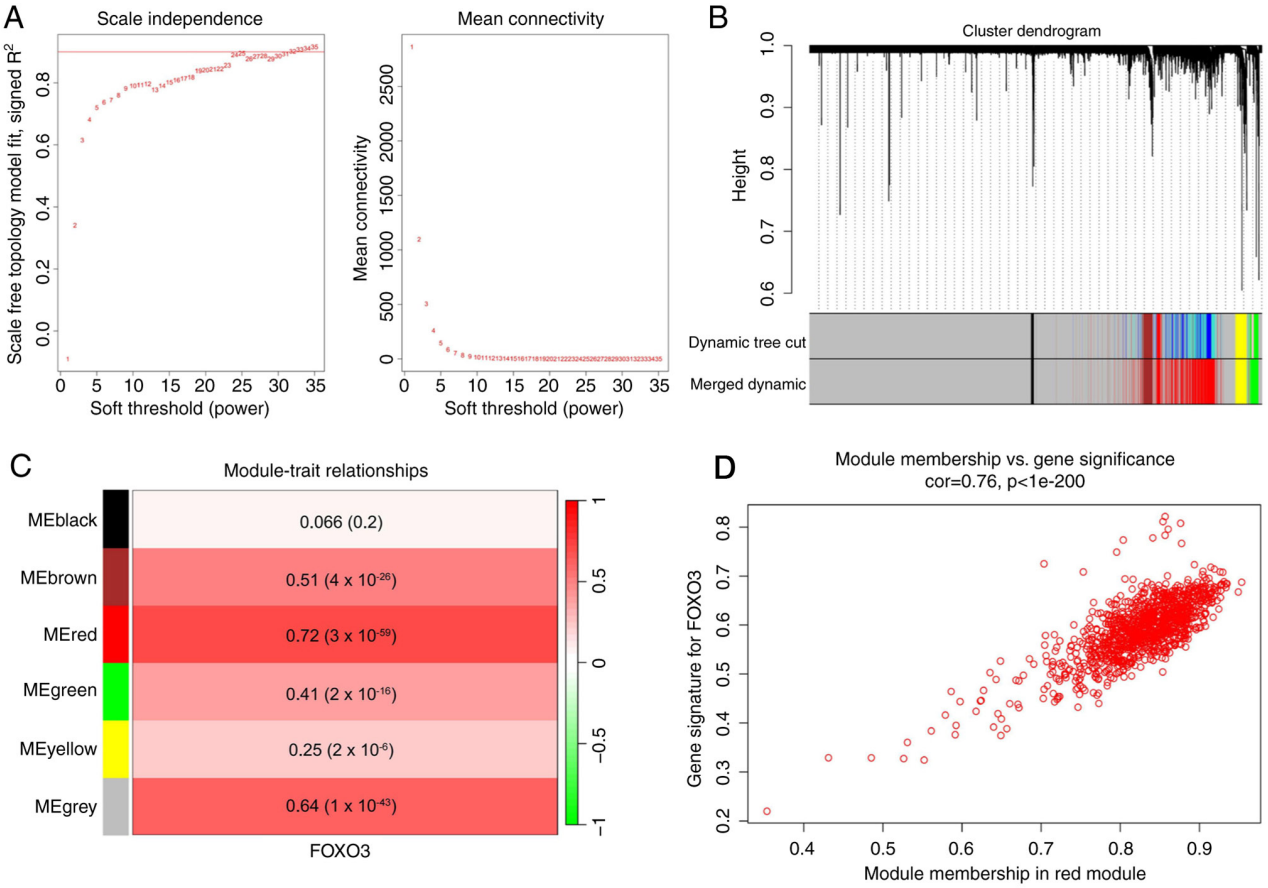

Figure 2. Weighted correlation network analysis of The Cancer Genome Atlas dataset. (A) Analysis of the scale-free index (left) and mean connectivity (right) for various soft-threshold powers (β). (B) Dendrogram of all differentially expressed genes clustered based on the measurement of dissimilarity (1-TOM). The color band shows the distribution of modules. (C) Heatmap of the correlation between the modules and mRNA expression of FOXO3 in HCC. The module with the highest coefficient was used for subsequent analysis. (D) Module membership vs. gene significance scatter plot of FOXO3. FOXO3, Forkhead box O3; HCC, hepatocellular carcinoma.

five genes (DDX55, TAF1B, TAF3, RAB10 and RAB7A) for constructing the model according to the minimum λ value (Fig. 3B and C). Fig. 3D shows the PPI network between FOXO3 and the 294 proteins obtained from univariate Cox regression analysis.

Construction and validation of a prognostic model based on the five genes. According to the results of LASSO regression analysis, the expression values and regression coefficients of these five genes for each sample were used to calculate the RS of each sample. Subsequently, the cut-off values of the RS were obtained using X-tile software and the patients were divided into high-risk and low-risk groups (Fig. 4A). All five genes were more highly expressed in the high-risk group and the patients with HCC in the high-risk group had a worse prognosis compared with the low-risk group (Fig. 4B). The time-dependent ROC curve showed that the area under the curve (AUC) values for 1, 3 and 5 years were 0.73, 0.69 and 0.71, respectively (Fig. 4C). ICGC data was used to evaluate the robustness of the model and similar results were obtained (Fig. 4D-F). Moreover, the present model was compared with other prognostic models which found the AUC values (1-year) of the present model were higher compared with the AUC values (1-year) of other models in training and validation sets (Table SII) (29-33).

RS potential to evaluate HCC prognosis. To further evaluate the clinical value of the model, univariate and multivariate Cox regression analyses were used to analyze the RS and other clinical factors (age, sex, TNM staging and vascular invasion) in both datasets. Both univariate Cox analysis (Fig. 5A and D) and multivariate Cox analysis (Fig. 5B and E) showed that RS and TNM staging were risk factors in both datasets. Considering that TNM staging has been accepted as a standard prognostic method, these results suggested that RS has potential for clinical prognostic evaluation. In addition, RS and TNM staging in TCGA and ICGC Cox analysis showed similar statistical significance, although TNM staging has a higher hazard ratio. However, age, sex and vascular invasion were statistically significant only in partial Cox analyses. TNM staging and RS were used to construct nomograms in both datasets to quantify prognostic scores for patients with HCC. For TCGA dataset, the survival probability of patients with HCC with total points >100 was <0.6 (Fig. 5C). Similarly, the 4-year survival probability of patients with HCC with total points >100 was <0.6 in the ICGC dataset (Fig. 5F). The calibration curves of TCGA and ICGC datasets are shown in Fig. S2.

Differences in the carcinogenic pathways and tumor microenvironment between high- and low-risk groups. Activation of carcinogenic pathways is an integral part of tumor progression (32). In HCC, tumor development is often accompanied

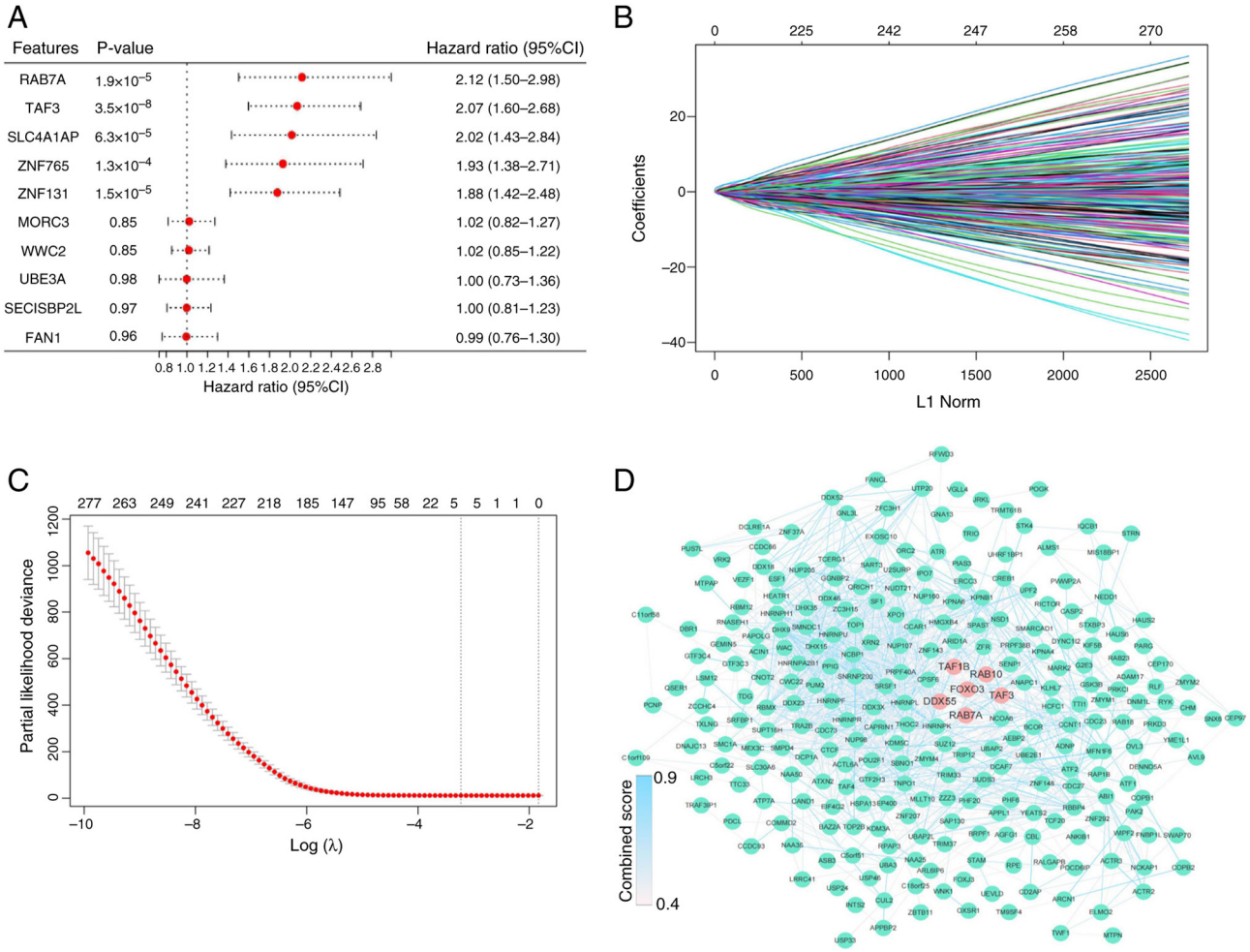

Figure 3. Identification of the 5-gene signature. (A) Forest plot of univariate Cox regression analysis in The Cancer Genome Atlas dataset. Cox results for the top five and bottom five genes. (B) Least absolute shrinkage and selection operator regression analysis. (C) λ curves show the least absolute shrinkage and the best λ was selected based on the minimum criteria. (D) The protein-protein interaction network between FOXO3 and 294 genes. FOXO3, DDX55, RAB10, RAB7A, TAF1B and TAF3 are highlighted by red dots and the remaining genes are represented by green dots. The color of the edges was determined by the combined score obtained from STRING. FOXO3, Forkhead box O3; DDX55, DEAD-box helicase 55; RAB10, RAB10, member RAS oncogene family; RAB7A, RAB7A, member RAS oncogene family; TAF1B, TATA-box binding protein associated factor, RNA polymerase I subunit B; TAF3, TATA-box binding protein associated factor 3; SLC4A1AP, solute carrier family 4 member 1 adaptor protein; ZNF765, zinc finger protein 765; MORC3, MORC family CW-type zinc finger 3; WWC2, WW and C2 domain containing 2; UBE3A, ubiquitin protein ligase E3A; SECISBP2L, SECIS binding protein 2 like; FAN1, FANCD2 And FANCI associated nuclease 1.

by activation of cell cycle-associated pathways and phosphorylation of the AKT pathway and the activity of these pathways suggests poor prognosis of patients (34). In the present study, GSEA was performed for patients in the high- and low-RS groups, which demonstrated that the cell cycle-associated pathways (G_2/M checkpoint and E2F targets) and AKT pathway were more active in the high-RS group (Fig. 6A-C), partly explaining why patients in the high-risk group had worse outcomes. Similar results were obtained from the ICGC dataset (Fig. S3A-C).

The tumor microenvironment, in which several immune cells play a major role, is another important factor mediating tumor prognosis (35). Thus, the infiltration of 22 immune cell types was quantified using transcriptome data from patients in the high- and low-risk groups. In TCGA and ICGC datasets, M2 macrophages and $CD4^+$ T cells were the main immune cells enriched in the tumor microenvironment (Figs. 6D and S3D). In addition, there was more infiltration of M2 macrophages and resting $CD4^+$ memory T cells in the high-risk group compared with the low-risk group in TCGA dataset (Fig. 6E). Compared with the high-risk groups, a higher infiltration of activated natural killer cells was found in the low-risk groups in TCGA and ICGC datasets (Figs. 6E and S3E).

Identification and validation of the 5-gene signature in HCC. The expression of the five genes (DDX55, RAB10, RAB7A, TAF1B and TAF3) used for constructing the model in HCC was further investigated. TCGA and ICGA datasets both showed that these five genes were highly expressed in HCC tissues compared with normal tissues (Figs. 7A and S4A). Moreover, the high expression of these five genes in TCGA dataset was significantly associated with poor prognosis of HCC, while only the expression of the RAB10, RAB7A and TAF3 genes was associated with poor prognosis of patients with HCC in the ICGC dataset (Figs. 7B-F and S4B-F). To validate these results, tumor and matched non-tumor tissues were collected from ten patients with HCC. The RT-qPCR analysis indicated that the mRNA expression of the five genes in tumor tissues was higher compared

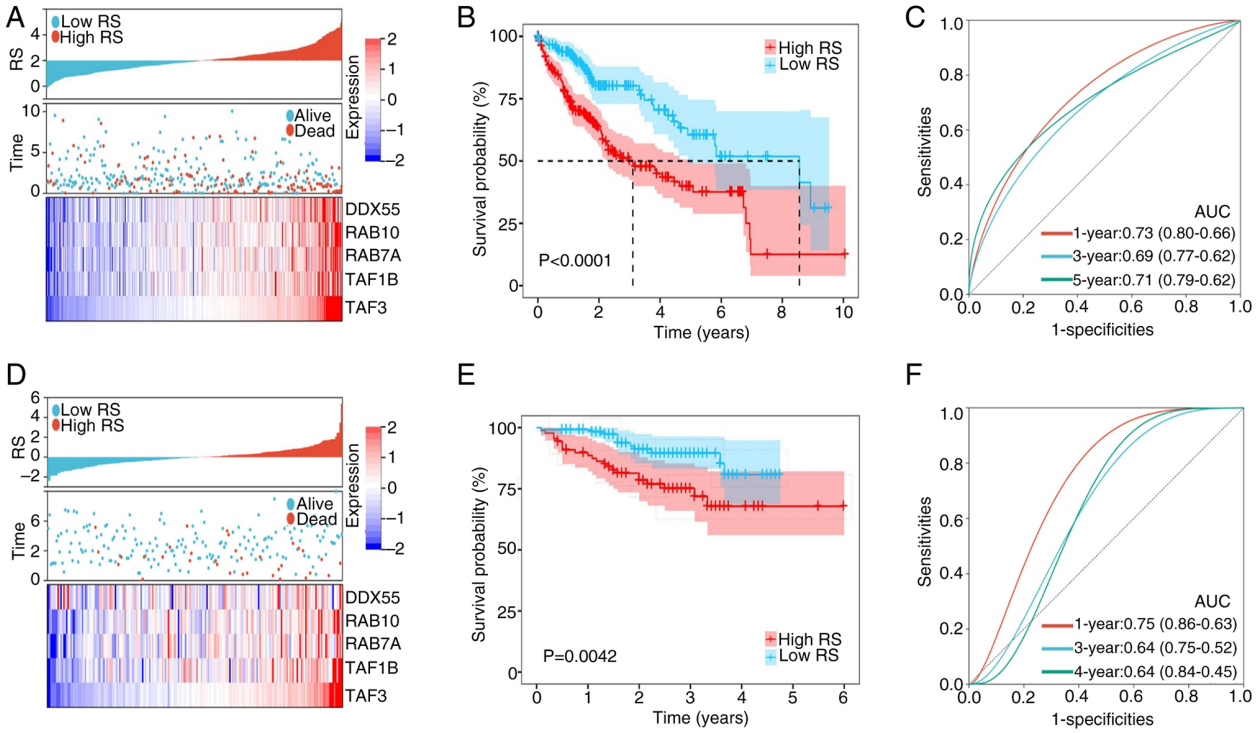

Figure 4. Construction and validation of a 5-gene prognostic model. (A) The distribution of RS, survival status and expression of the 5-gene signature between the high- and low-risk groups in TCGA dataset. (B) Overall survival of patients with HCC in the high- and low- RS groups in TCGA dataset. (C) Time-dependent ROC curve of RS in TCGA dataset. (D) The distribution of RS, survival status and expression of the 5-gene signature between the high- and low-risk groups in the ICGC dataset. (E) Overall survival of patients with HCC in the high- and low-RS groups in the ICGC dataset. (F) Time-dependent ROC curve of RS in the ICGC dataset. RS, risk score; TCGA, The Cancer Genome Atlas; ICGC, International Cancer Genome Consortium; ROC, receiver operating characteristic; DDX55, DEAD-box helicase 55; RAB10, RAB10, member RAS oncogene family; RAB7A, RAB7A, member RAS oncogene family; TAF1B, TATA-box binding protein associated factor, RNA polymerase I subunit B; TAF3, TATA-box binding protein associated factor 3; AUC, area under the curve.

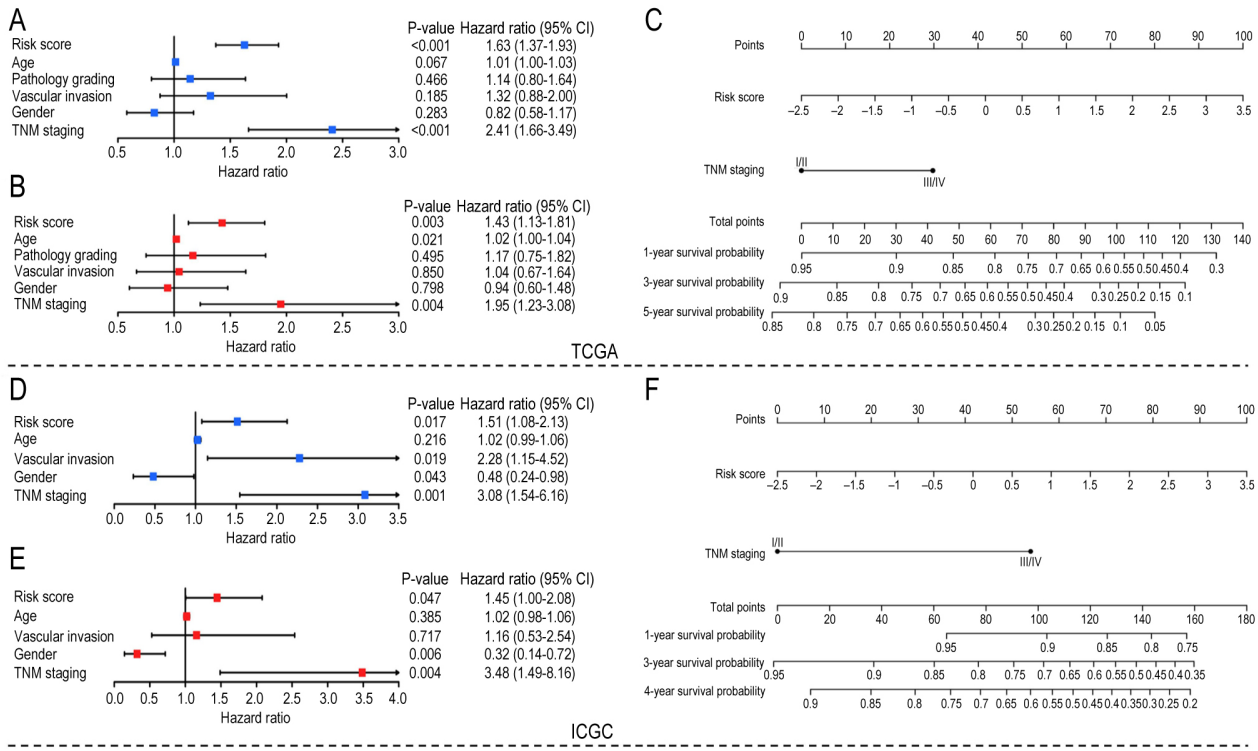

Figure 5. Clinical potential of the RS for prognosis. (A) Univariate and (B) multivariate Cox analyses of the RS and other clinical factors in TCGA dataset. (C) Nomogram of TNM staging and RS based on the Cox results in TCGA dataset. (D) Univariate and (E) multivariate Cox analyses of the RS and other clinical factors in the ICGC dataset. (F) Nomogram of TNM staging and RS based on the Cox results in the ICGC dataset. RS, risk score; TCGA, The Cancer Genome Atlas; ICGC, International Cancer Genome Consortium; TNM, tumor, node, metastasis.

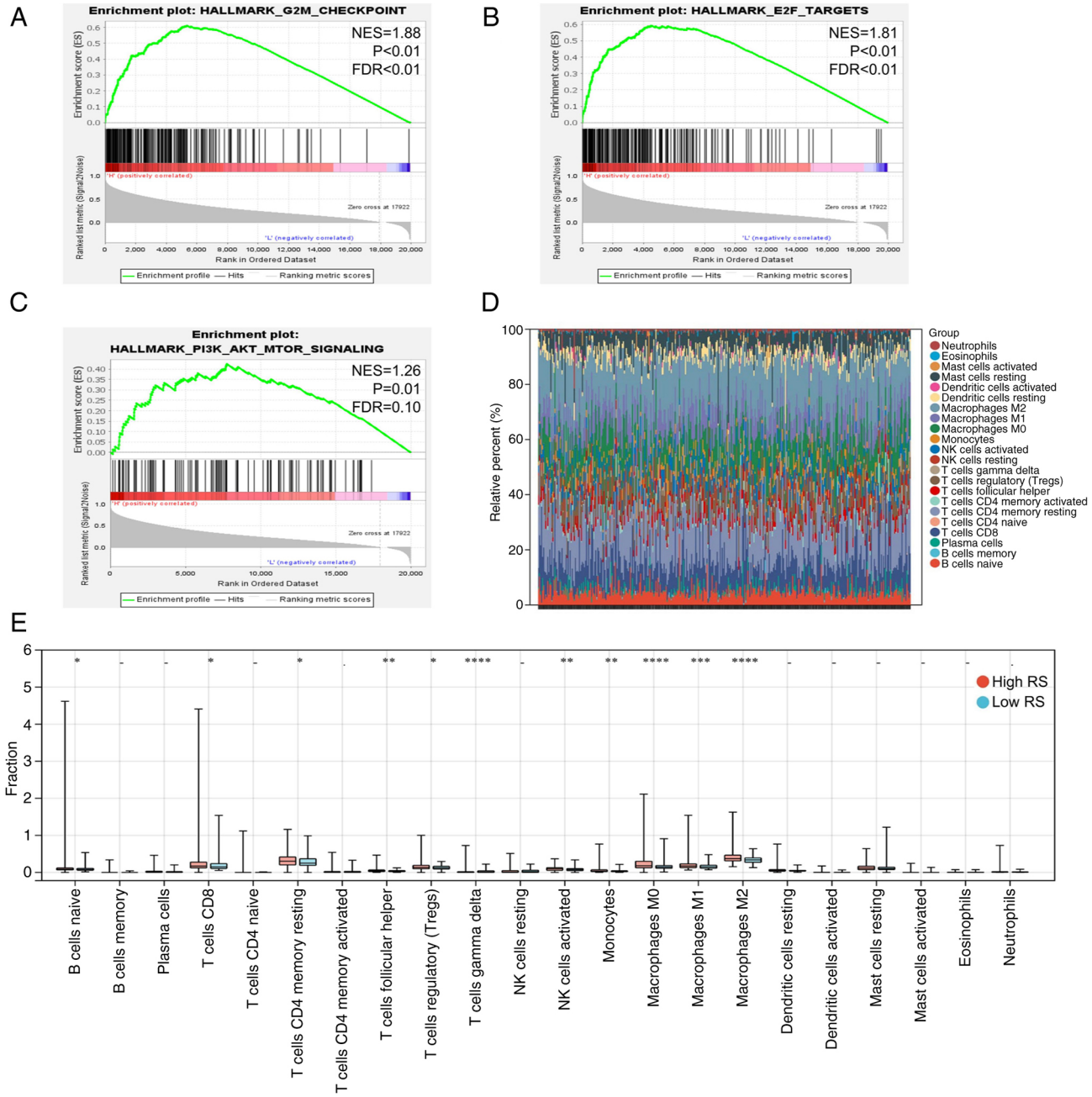

Figure 6. Analyses of the carcinogenic pathways and tumor microenvironment between the high- and low-RS groups in The Cancer Genome Atlas dataset. Gene set enrichment analysis of the high-RS group vs. the low-RS group for (A) the G_2/M checkpoint, (B) E2F targets and (C) PI3K/AKT/MTOR signaling. (D) Distribution of 22 immune cell types in the tumor microenvironment of each hepatocellular carcinoma sample. (E) Comparison of 22 immune cell types infiltrated in tumor microenvironment between the high- and low-RS groups. -, not significant; *P<0.05; **P<0.01; ***P<0.001; ****P<0.0001. RS, risk score; FDR, false discovery rate; NES, normalized enrichment score.

with that in non-tumor tissues (Fig. 7G). Immunohistochemical results from the Human Protein Atlas (HPA) database suggested that DDX55, RAB10 and RAB7A have higher expression in tumor tissue compared with non-tumor tissue (Fig. 7H) (36). However, it was not possible to obtain representative immunohistochemical staining results for TAF1B and TAF3 from the HPA database. Western blot analysis demonstrated that there was higher protein expression levels of all five proteins in tumor tissues compared with non-tumor tissues (Fig. 7I).

To further explore the influence of the genes of interest on HCC progression, three genes (RAB10, RAB7A and TAF3) that were significantly associated with prognosis in both TCGA and ICGC datasets were selected for functional experiments. The CCK-8 assay demonstrated that knockdown of RAB10, RAB7A and TAF3 inhibited the proliferation of Huh7 cells (Figs. 7J and S4G). Moreover, the AUC values (1-year) among five genes, RS and TNM in TCGA and ICGC datasets were compared which demonstrated the five genes and RS were not inferior to TNM in predicting first-year survival status of patients with HCC (Fig. S5A and B). In addition, the protein expression of FOXO3 was knocked down using siRNA (Fig. S5C). The protein expression levels of the other five proteins (DDX55, RAB10, RAB7A, TAF3 and TAF1B) were also downregulated after knocking down FOXO3 (Fig. S5D).

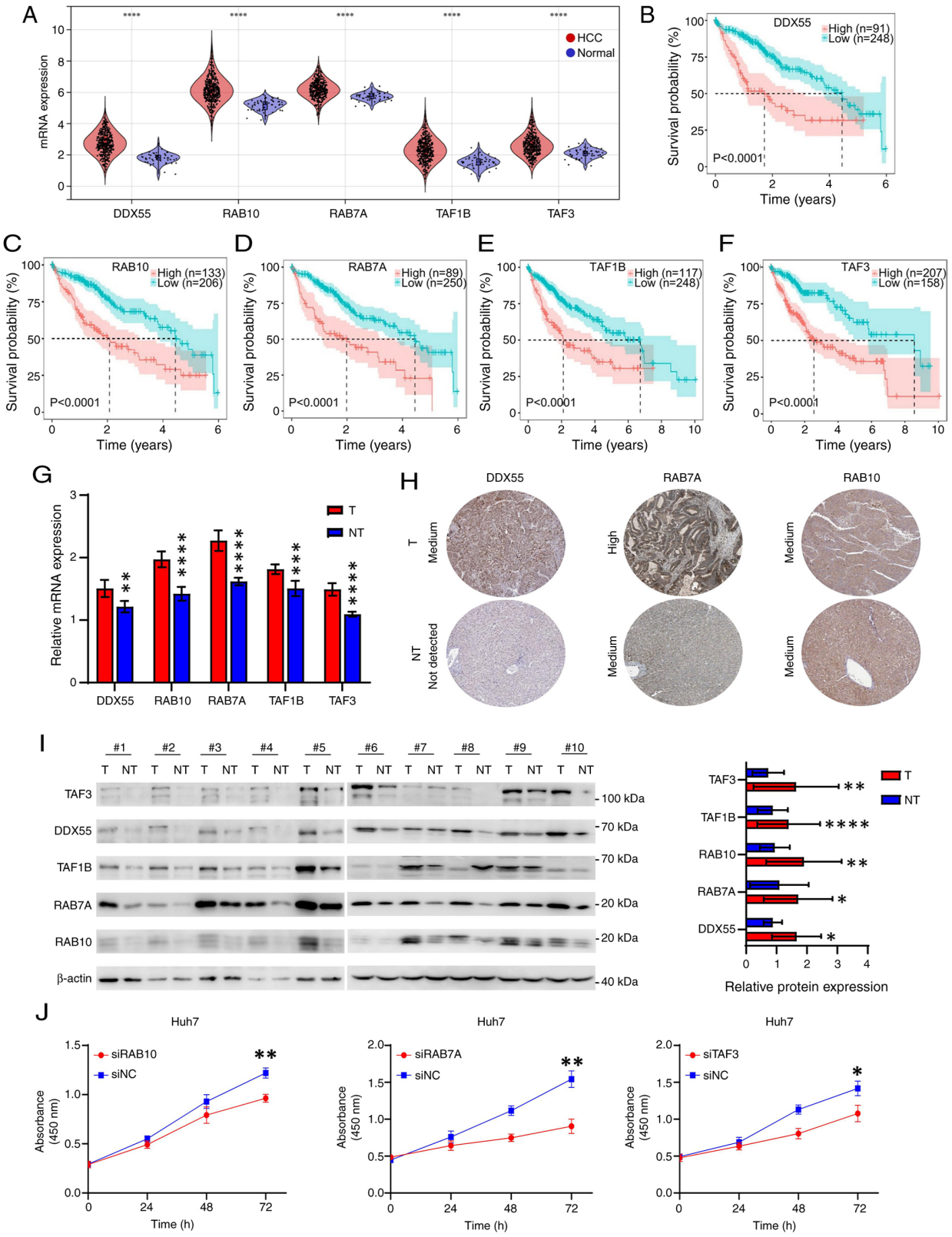

Figure 7. Identification of five biomarkers in HCC. (A) mRNA expression of DDX55, RAB10, RAB7A, TAF1B and TAF3 in HCC and normal tissues from TCGA. Overall survival curves in patients with HCC with high or low expression of (B) DDX55, (C) RAB10, (D) RAB7A, (E) TAF1B and (F) TAF3 from TCGA dataset. The best cut-off value for each gene was obtained using the X-tile software. (G) mRNA expression of DDX55, RAB10, RAB7A, TAF1B and TAF3 in HCC and paired paracancerous tissues from 10 patients with HCC, assessed using reverse transcription-quantitative PCR. (H) Immunohistochemical images of DDX55, RAB10 and RAB7A in HCC and normal tissues obtained from the HPA. (I) Protein expression of DDX55, RAB10, RAB7A, TAF1B and TAF3 in HCC and paired paracancerous tissues from 10 patients with HCC, evaluated using western blot analysis. The figure on the right is a relative semi-quantitative histogram of protein expression. The gray values were obtained by ImageJ and analyzed using GraphPad Prism. (J) Cell Counting Kit-8 curves after knockdown of RAB10, RAB7A and TAF3 in Huh7 cells by siRNA. *P<0.05; **P<0.01; ***P<0.001; ****P<0.0001. T, tumor; NT, not-tumor; HCC, hepatocellular carcinoma; TCGA, The Cancer Genome Atlas; DDX55, DEAD-box helicase 55; RAB10, RAB10, member RAS oncogene family; RAB7A, RAB7A, member RAS oncogene family; TAF1B, TATA-box binding protein associated factor, RNA polymerase I subunit B; TAF3, TATA-box binding protein associated factor 3; HPA, The Human Protein Atlas; NC, negative control.

Additionally, mRNA levels of FOXO3 were positively correlated with mRNA levels of the 5 genes in both TCGA and ICGA datasets (Fig. S6).

Discussion

The FOXO protein has four subtypes, FOXO1, FOXO3, FOXO4 and FOXO6 (8). The distribution of the four subtypes is different: FOXO1 is highly expressed in fat cells, FOXO4 is highly expressed in muscle cells and FOXO6 is highly expressed in brain tissue. Only FOXO3 is highly expressed in hepatocytes (9). Previous studies have focused on FOXO3 as the downstream effector of several tumor-associated pathways (such as AKT and AMP-activated protein kinase) to mediate the development of tumors. However, further exploration is needed for downstream targets of FOXO3. Currently, the role of FOXO3 in HCC is controversial (16-18). The present study revealed that FOXO3 was highly expressed in HCC tissue and indicated a poor prognosis. Bioinformatics analysis identified five FOXO3-associated genes (DDX55, RAB10, RAB7A, TAF1B and TAF3). The training and validation sets confirmed the robustness and clinical potential of the prognostic model. Subtypes analysis indicated that patients with HCC in the high-risk group had significantly more active carcinogenic pathways and tumor microenvironment. Moreover, RAB10, RAB7A and TAF3 were identified as potential genes involved in tumor development.

WGCNA combined with LASSO to construct prognostic models and molecular typing have previously been used for colorectal and liver cancer (37-42). For example, a 4-signature model based on the scRNA-seq and bulk RNA-seq data could evaluate the prognostic risk of patients with colorectal cancer. Similarly, a prognostic model based on the SMG5 and MRPL9 genes predicted the tumor mutation burden of HCC patients. The advantage of public databases is that they have large-scale open information of clinical samples and gene expression profiles and the utilization of these resources has promoted the development of molecular diagnostic and prognostic models in the field of cancer. An increasing number of prognostic models and molecular typing methods have been developed in HCC and some sequencing studies based on large-scale new clinical HCC samples have supported the potential use of bioinformatics in tumor prognosis assessment (4-6,40). Compared with models of the same modeling method, the model in the present study had fewer signatures, which was conducive to the translation of the model to the clinic. Additionally, in the external validation set (not including the internal validation set from the same database), the present model had significantly improved AUC values in the first year compared with other models. The subsequent 3-year and 5-year AUC values also had a slight advantage, suggesting that the present model has improved robustness compared with other models. Notably, the Cox analysis results showed some differences in clinical features (TNM, sex and vascular invasion) between the two datasets. This is potentially due to the high heterogeneity of HCC; specifically, clinical features, heterogeneous gene expression and sample size may cause these differences between the TCGA and ICGC cohorts. However, these differences did not affect the conclusions of the present study because intersections were taken in both datasets.

The present study identified and confirmed three genes, RAB10, RAB7A and TAF3, with potential as biomarkers. Knockdown of RAB10 inhibits the proliferation of HCC cells *in vivo* and *in vitro* and is accompanied by downregulated activity of multiple carcinogenic pathways (such as AKT, insulin receptor and AXL receptor tyrosine kinase) (42). O-GlcNAcylation of RAB10 has also been reported to promote HCC progression (43). Similarly, RAB7A is upregulated in HCC and overexpression of RAB7A promotes tumor proliferation and metastatic potential (44). Mechanistically, RAB7A regulates the activity of the AKT pathway and the expression of cycle-associated proteins [cyclin dependent kinase (CDK) 4, CDK6 and cyclin A2]. Consistently, the present GSEA suggested that the difference in prognosis among patients with HCC is attributed to the activity of AKT and cell cycle-associated pathways. Furthermore, as FOXO3 activates the AKT pathway, the results suggested RAB7A may be an important effector by which FOXO3 regulated the AKT pathway. TAF3 serves an important role in the differentiation of embryonic stem cells and in finely balanced transcription programs (45). To date, the role and molecular mechanism of TAF3 in HCC have not been reported. RAB10 and RAB7A have been demonstrated to serve pro-cancerous roles in HCC, and the present results classified RAB10, RAB7A and TAF3 as FoxO3-related genes. Thus, we speculate that TAF3 may also have a similar functional role and be involved in HCC progression. In addition, DDX55 promotes HCC proliferation and metastasis by interacting with bromodomain-containing protein 4 and TAF1B depletion induces HCC cell apoptosis via nucleolar stress and activation of the p53/miR-101 circuit (46,47). The present study revealed a correlation between FOXO3 and the 5 signature genes (DDX55, RAB10, RAB7A, TAF1B and TAF3), which set the direction for subsequent FOXO3 target exploration. However, our results only indicate that FOXO3 is associated with these genes and interferes with their expression. Whether this regulatory association of FOXO3 is direct or indirect remains to be verified by further experiments.

Although the present study deepened the understanding of FOXO3 in HCC, exploring novel potential related molecules and a novel prognostic model, there remain limitations. First, the present study lacked more clinical samples for multi-omics, FOXO3 expression verification and prognosis assessment in patients with HCC. The differences in RS, TNM stage, age, sex and vascular invasion in the TCGA and ICGC Cox analyses might be caused by the HCC heterogeneity and ethnicity. Second, the present study still needs more direct and clinical evidence to validate the model and the intermolecular links. Nevertheless, it provided guidance for follow-up research, including relevant clinical work and basic experiments, which are the focus of our future work.

For the first time, to the best of the authors' knowledge, the present study constructed a novel prognostic model based on FOXO3 and identified a novel 5-gene signature. The potential of three genes as biomarkers in HCC was confirmed, including the novel TAF3 biomarker. Future research will

investigate the roles and underlying molecular mechanisms of TAF3 in HCC. In future clinical practice, pathological and molecular detection methods can be used to assess the expression of relevant genes and score them into the model to evaluate the prognosis of the patient. We hypothesize that this is the most important and widespread use of prognostic models. In summary, the present study constructed a novel FOXO3-associated prognostic model and validated three major genes through biochemical experimental studies. The present results complement the bioinformatics findings for the molecular typing and prognosis of HCC, further improving the understanding of the roles of FOXO3, RAB10, RAB7A and TAF3 in HCC.

Acknowledgements

Not applicable.

Funding

The present study was supported by the Zhanjiang Science and Technology Development Special Projects (grant nos. 2021A05101 and 2022A01147), the Second Affiliated Hospital of Guangdong Medical University (grant no. 21H03) in 2021 and the Research Project of Guangdong Traditional Chinese Medicine Bureau (grant no. 20221439) in 2022.

Availability of data and materials

The data generated in the present study may be requested from the corresponding author.

Authors' contributions

The present study was conceived and designed by SG, QL and SD. Data collection and bioinformatics analysis were performed by SG, QL and PH. SG, QL, PH and KL analyzed and interpreted data. The manuscript was written and revised by SG and SD. SD was responsible for supervision of the whole project. SG and SD confirm the authenticity of all the raw dada. All authors read and approved the final version of the manuscript.

Ethics approval and consent to participate

In the present study, the confidentiality of patient information was guaranteed using a de-identified and anonymous method. Moreover, the utilization of public databases involving human data was reviewed and approved by the Ethics Committee of The Second Affiliated Hospital of Guangdong Medical University (PJKT-2024-042). Written informed consent was obtained from all participants.

Patient consent for publication

Not applicable.

Competing interests

The authors declare that they have no competing interests.

References

1. Sung H, Ferlay J, Siegel RL, Laversanne M, Soerjomataram I, Jemal A and Bray F: Global cancer statistics 2020: GLOBOCAN estimates of incidence and mortality worldwide for 36 cancers in 185 countries. CA Cancer J Clin 71: 209-249, 2021.
2. Yang JD, Hainaut P, Gores GJ, Amadou A, Plymoth A and Roberts LR: A global view of hepatocellular carcinoma: Trends, risk, prevention and management. Nat Rev Gastroenterol Hepatol 16: 589-604, 2019.
3. Llovet JM, Pinyol R, Kelley RK, El-Khoueiry A, Reeves HL, Wang XW, Gores GJ and Villanueva A: Molecular pathogenesis and systemic therapies for hepatocellular carcinoma. Nat Cancer 3: 386-401, 2022.
4. Wang T, Dang N, Tang G, Li Z, Li X, Shi B, Xu Z, Li L, Yang X, Xu C and Ye K: Integrating bulk and single-cell RNA sequencing reveals cellular heterogeneity and immune infiltration in hepatocellular carcinoma. Mol Oncol 16: 2195-2213, 2022.
5. Zhang Q, Lou Y, Yang J, Wang J, Feng J, Zhao Y, Wang L, Huang X, Fu Q, Ye M, *et al*: Integrated multiomic analysis reveals comprehensive tumour heterogeneity and novel immunophenotypic classification in hepatocellular carcinomas. Gut 68: 2019-2031, 2019.
6. Ho DW, Tsui YM, Chan LK, Sze KM, Zhang X, Cheu JW, Chiu YT, Lee JM, Chan AC, Cheung ET, *et al*: Single-cell RNA sequencing shows the immunosuppressive landscape and tumor heterogeneity of HBV-associated hepatocellular carcinoma. Nat Commun 12: 3684, 2021.
7. Kim E and Viatour P: Hepatocellular carcinoma: Old friends and new tricks. Exp Mol Med 52: 1898-1907, 2020.
8. Orea-Soufi A, Paik J, Bragança J, Donlon TA, Willcox BJ and Link W: FOXO transcription factors as therapeutic targets in human diseases. Trends Pharmacol Sci 43: 1070-1084, 2022.
9. Calissi G, Lam EWF and Link W: Therapeutic strategies targeting FOXO transcription factors. Nat Rev Drug Discov 20: 21-38, 2021.
10. Galili N, Davis RJ, Fredericks WJ, Mukhopadhyay S, Rauscher FJ, Emanuel BS, Rovera G and Barr FG: Fusion of a fork head domain gene to PAX3 in the solid tumour alveolar rhabdomyosarcoma. Nat Genet 5: 230-235, 1993.
11. Davis RJ, D'Cruz CM, Lovell MA, Biegel JA and Barr FG: Fusion of PAX7 to FKHR by the variant t(1;13)(p36;q14) translocation in alveolar rhabdomyosarcoma. Cancer Res 54: 2869-2872, 1994.
12. Dansen TB and Burgering BMT: Unravelling the tumor-suppressive functions of FOXO proteins. Trends Cell Biol 18: 421-429, 2008.
13. Link W and Fernandez-Marcos PJ: FOXO transcription factors at the interface of metabolism and cancer. Int J Cancer 141: 2379-2391, 2017.
14. Paik JH, Kollipara R, Chu G, Ji H, Xiao Y, Ding Z, Miao L, Tothova Z, Horner JW, Carrasco DR, *et al*: FoxOs are lineage-restricted redundant tumor suppressors and regulate endothelial cell homeostasis. Cell 128: 309-323, 2007.
15. Hu T, Chung YM, Guan M, Ma M, Ma J, Berek JS and Hu MCT: Reprogramming ovarian and breast cancer cells into non-cancerous cells by low-dose metformin or SN-38 through FOXO3 activation. Sci Rep 4: 5810, 2014.
16. Liang C, Chen W, Zhi X, Ma T, Xia X, Liu H, Zhang Q, Hu Q, Zhang Y, Bai X and Liang T: Serotonin promotes the proliferation of serum-deprived hepatocellular carcinoma cells via upregulation of FOXO3a. Mol Cancer 12: 14, 2013.
17. Yao J, WANG J, Xu Y, Guo Q, Sun Y, Liu J, Li S, Guo Y and Wei L: CDK9 inhibition blocks the initiation of PINK1-PRKN-mediated mitophagy by regulating the SIRT1-FOXO3-BNIP3 axis and enhances the therapeutic effects involving mitochondrial dysfunction in hepatocellular carcinoma. Autophagy 18: 1879-1897, 2022.
18. Yang LJ, Tang Q, Wu J, Chen Y, Zheng F, Dai Z and Hann SS: Inter-regulation of IGFBP1 and FOXO3a unveils novel mechanism in ursolic acid-inhibited growth of hepatocellular carcinoma cells. J Exp Clin Cancer Res 35: 59, 2016.
19. Lin Z, Niu Y, Wan A, Chen D, Liang H, Chen X, Sun L, Zhan S, Chen L, Cheng C, *et al*: RNA m6A methylation regulates sorafenib resistance in liver cancer through FOXO3-mediated autophagy. EMBO J 39: e103181, 2020.
20. Colaprico A, Silva TC, Olsen C, Garofano L, Cava C, Garolini D, Sabedot TS, Malta TM, Pagnotta SM, Castiglioni I, *et al*: TCGAbiolinks: An R/bioconductor package for integrative analysis of TCGA data. Nucleic Acids Res 44: e71, 2016.

21. Langfelder P and Horvath S: WGCNA: An R package for weighted correlation network analysis. BMC Bioinformatics 9: 559, 2008.
22. Friedman J, Hastie T and Tibshirani R: Regularization paths for generalized linear models via coordinate descent. J Stat Softw 33: 1-22, 2010.
23. Shi Y, Wang Y, Dong H, Niu K, Zhang W, Feng K, Yang R and Zhang Y: Crosstalk of ferroptosis regulators and tumor immunity in pancreatic adenocarcinoma: Novel perspective to mRNA vaccines and personalized immunotherapy. Apoptosis 28: 1423-1435, 2023.
24. Zhang G, Su L, Lv X and Yang Q: A novel tumor doubling time-related immune gene signature for prognosis prediction in hepatocellular carcinoma. Cancer Cell Int 21: 522, 2021.
25. Robin X, Turck N, Hainard A, Tiberti N, Lisacek F, Sanchez JC and Muller M: pROC: An open-source package for R and S+ to analyze and compare ROC curves. BMC Bioinformatics 12: 77, 2011.
26. Ito K and Murphy D: Application of ggplot2 to pharmacometric graphics. CPT Pharmacometrics Syst Pharmacol 2: e79, 2013.
27. Abe S, Kawa K, Nozawa H, Hata K, Kiyomatsu T, Tanaka T, Nishikawa T, Otani K, Sasaki K, Kaneko M, *et al*: Use of a nomogram to predict the closure rate of diverting ileostomy after low anterior resection: A retrospective cohort study. Int J Surg 47: 83-88, 2017.
28. Livak K and Schimittgen T: Analysis of relative gene expression data using real-time quantitive PCR and the 2 (-delata delta C(T)) method. Methods 25: 402-408, 2001.
29. Zhang Z, Zeng X, Wu Y, Liu Y, Zhang X and Song Z: Cuproptosis-related risk score predicts prognosis and characterizes the tumor microenvironment in hepatocellular carcinoma. Front Immunol 13: 925618, 2022.
30. Tang Y, Xu L, Ren Y, Li Y, Yuan F, Cao M, Zhang Y, Deng M and Yao Z: Identification and validation of a prognostic model based on three MVI-related genes in hepatocellular carcinoma. Int J Biol Sci 18: 261-275, 2022.
31. Tian Z, Song J, She J, He W, Guo S and Dong B: Constructing a disulfidptosis-related prognostic signature of hepatocellular carcinoma based on single-cell sequencing and weighted co-expression network analysis. Apoptosis 29: 1632-1647, 2024.
32. Pu Q, Yu L, Liu X, Yan H, Xie Y, Cai X, Wu Y, Du J and Yang Z: Prognostic value of CD8+T cells related genes and exhaustion regulation of Notch signaling pathway in hepatocellular carcinoma. Front Immunol 15: 1375864, 2024.
33. Peng L, Xu S and Xu JL: Integration of single-cell RNA sequencing and bulk RNA sequencing to identify an immunogenic cell death-related 5-gene prognostic signature in hepatocellular carcinoma. J hepatocell Carcinoma 11: 879-900, 2024.
34. Moeini A, Cornellà H and Villanueva A: Emerging signaling pathways in hepatocellular carcinoma. Liver Cancer 1: 83-93, 2012.
35. Wang G, Wang Q, Liang N, Xue H, Yang T, Chen X, Qiu Z, Zeng C, Sun T, Yuan W, *et al*: Oncogenic driver genes and tumor microenvironment determine the type of liver cancer. Cell Death Dis 11: 313, 2020.
36. Uhlen M, Fagerberg L, Hallstrom B, Lindskog C, Oksvold P, Mardinoglu A, Sivertsson A, Kampf C, Sjostedt E, Asplund A, *et al*: Proteomics. Tissue-based map of the human proteome. Science 23: 347, 2015.
37. Cheng K, Cai N, Zhu J, Yang X, Liang H and Zhang W: Tumor-associated macrophages in liver cancer: From mechanisms to therapy. Cancer Commun (Lond) 42: 1112-1140, 2022.
38. Di Z, Zhou S, Xu G, Ren L, Li C, Ding Z, Huang K, Liang L and Yuan Y: Single-cell and WGCNA uncover a prognostic model and potential oncogenes in colorectal cancer. Biol Proced Online 24: 13, 2022.
39. Lu J, Chen Y, Zhang X, Guo J, Xu K and Li L: A novel prognostic model based on single-cell RNA sequencing data for hepatocellular carcinoma. Cancer Cell Int 22: 38, 2022.
40. Zhao Z, He S, Yu X, Lai X, Tang S, Mariya M EA, Wang M, Yan H, Huang X, Zeng S and Zha D: Analysis and experimental validation of rheumatoid arthritis innate immunity gene CYFIP2 and pan-cancer. Front Immunol 13: 954848, 2022.
41. Tang B, Zhu J, Zhao Z, Lu C, Liu S, Fang S, Zheng L, Zhang N, Chen M, Xu M, *et al*: Diagnosis and prognosis models for hepatocellular carcinoma patient's management based on tumor mutation burden. J Adv Res 33: 153-165, 2021.
42. Wang W, Jia WD, Hu B and Pan YY: RAB10 overexpression promotes tumor growth and indicates poor prognosis of hepatocellular carcinoma. Oncotarget 8: 26434-26447, 2017.
43. Lv Z, Ma G, Zhong Z, Xie X, Li B and Long D: O-GlcNAcylation of RAB10 promotes hepatocellular carcinoma progression. Carcinogenesis 44: 785-794, 2023.
44. Liu Y, Ma J, Wang X, Liu P, Cai C, Han Y, Zeng S, Feng Z and Shen H: Lipophagy-related gene RAB7A is involved in immune regulation and malignant progression in hepatocellular carcinoma. Comput Biol Med 158: 106862, 2023.
45. Liu Z, Scannell DR, Eisen MB and Tjian R: Control of embryonic stem cell lineage commitment by core promoter factor, TAF3. Cell 146: 720-731, 2011.
46. Yu B, Zhou S, Long D, Ning Y, Yao H, Zhou E and Wang Y: DDX55 promotes hepatocellular carcinoma progression by interacting with BRD4 and participating in exosome-mediated cell-cell communication. Cancer Sci 113: 3002-3017, 2022.
47. Chen HF, Gao DD, Jiang XQ, Sheng H, Wu Q, Zheng Q, Zhai QC, Yuan L, Liu M, Xu LF, *et al*: TAF1B depletion leads to apoptotic cell death by inducing nucleolar stress and activating p53-miR-101 circuit in hepatocellular carcinoma. Front Oncol 13: 1203775, 2023.